An investigation of the phase transitions in bornite (Cu$_5$FeS$_4$) using neutron diffraction and differential scanning calorimetry

Benjamin A. Grguric,[1,*] **Andrew Putnis,**[2,†] **and Richard J. Harrison**[2]

[1]Department of Earth Sciences, University of Cambridge, Downing Street, Cambridge CB2 3EQ, U.K.
[2]Institut für Mineralogie, Universität Münster, Corrensstrasse 24, D-48149 Münster, Germany

Abstract

Bornite (Cu$_5$FeS$_4$) exists in three polymorphic forms related by superstructuring, with structural transitions at 200 and 265 °C. The phase transitions and structural behavior in two natural bornite samples were investigated as a function of temperature using differential scanning calorimetry (DSC) to characterize the thermal anomalies associated with each transition and in-situ high-resolution neutron powder diffraction to determine the variation in superlattice intensity and lattice parameters. These two methods, carried out over the temperature range 50–350 °C, provided insight into the short- and long-range interactions, respectively, and a comparison of measurements taken up-T and down-T enabled thermal hysteresis effects to be quantified. The high to intermediate transition at 265 °C involves long-range cation ordering and vacancy clustering, resulting in a doubling of the high-temperature cubic unit cell ($m3m$). The square of both the spontaneous strain and the $2a$ superlattice intensity varied linearly with temperature, indicating that the transition is tricritical in character. Loss of long- and short-range order occurred simultaneously during heating, whereas during cooling, the reappearance of $2a$ superlattice reflections was depressed some 50 °C below the short-range transition recorded by DSC due to the formation of antiphase domains. The presence of antiphase domains also caused the discontinuity in the strain associated with the transition to occur at a different temperature to the appearance of superlattice intensity. The intermediate-low transition associated with the development of a $2a4a2a$ orthorhombic superlattice ($Pbca$) is strongly first-order and exhibits a large intrinsic hysteresis (38 °C). The down-T transition temperature of the intermediate-low transition is shown to be dependent on the degree of order attained in the intermediate phase.

Introduction

Bornite, Cu$_5$FeS$_4$, is an important copper ore mineral of widespread occurrence in various geological settings. Polymorphism and the associated structural phase transitions in this mineral have been the subject of numerous crystallographic studies since Frueh (1950) noted a temperature-dependent transition. Bornite has three temperature-dependent polymorphs, termed high, intermediate, and low. The intermediate and low forms can be described as superstructures of the high-temperature cubic form ($a = 5.5$ Å), the various superstructures arising from an increase in the ordering of vacancies and metal atoms with reducing temperature (Koto and Morimoto 1975; Putnis and Grace 1976; Pierce and Buseck 1978).

The high-temperature polymorph, stable above approximately 270 °C, consists of a random distribution of six metal cations and two vacancies in the eight tetrahedral interstices of a cubic close-packed sulfur framework

(Morimoto and Kullerud 1961, 1966; Kanazawa et al. 1978). This phase, which has the antifluorite-type structure (space group $Fm3m$), inverts to the intermediate form on rapid quenching (Morimoto 1964).

The intermediate polymorph exists over the temperature range 200–270 °C (Kanazawa et al. 1978; Grguric et al. 1996a and 1996b), with some variation induced by minor deviations from stoichiometry (Grguric and Putnis 1998). This cubic ($Fm3m$) structure constrains two alternating a sub-cells along the three crystallographic axes, resulting in a $2a$ superstructure. Kanazawa et al. (1978) denoted the two sub-cells M1 and M2 cubes, which differ from the high phase in their distribution of metal atoms and vacancies. M1 cubes have a disordered arrangement of four copper atoms and four metal vacancies, but M2 cubes have all eight tetrahedral sites filled with a random distribution of copper and iron atoms. Thus, the transition from the high to intermediate form involves a long-range vacancy clustering and cation ordering process, while retaining the close-packed sulfur framework of the high form. Kanazawa et al. (1978) demonstrated that metal atoms in the intermediate structure are not in regular tet-

---

* Present address: WMC Mount Keith Operations, P.O. Box 238, Welshpool Delivery Centre, W.A. 6986, Australia.
† E-mail: putnis@nwz.uni-muenster.de

rahedral coordination but are displaced toward the triangular faces of the sulfur tetrahedra.

The structure of the low polymorph, which exists below approximately 200 °C (Kanazawa et al. 1978; Grguric et al. 1996a and 1996b), was determined by Koto and Morimoto (1975) using Patterson methods to refine single-crystal X-ray data. The transition from the intermediate to the low form involves a doubling of the intermediate unit cell in the *b* direction, resulting in an orthorhombic (pseudo-tetragonal) $2a4a2a$ superstructure with cell dimensions $a = 10.950$ Å, $b = 21.862$ Å, $c = 10.950$ Å, and space group *Pbca*. This transition is postulated to result from ordering of the four vacancies in each of the M1 cubes into a tetrahedral arrangement as in the zinc-blend structure (Koto and Morimoto 1975; Pierce and Buseck 1978). The orientation of this vacancy tetrahedron alternates along the *b* axis in each M1 type cube, resulting in a $4a$ repeat of the unit cell along the orthorhombic *b* axis (Koto and Morimoto 1975; Kanazawa et al. 1978; Pierce and Buseck 1978). The four metal atoms in the zinc-blend type M1 cubes remain displaced from the centers of the tetrahedra. In the anti-fluorite type M2 cubes the metal atoms have more regular tetrahedral coordination. Because there are problems in distinguishing Cu from Fe atoms using X-ray methods in these studies it was not clear whether these metals are fully ordered in the M2 cubes of the low structure. Koto and Morimoto (1975) assigned Fe to two of the metal sites in the M2 cubes, M(4) and M(5), on the basis that these sites were the most regular of the tetrahedral sites. In the Rietveld refinements of the low structure using neutron powder diffraction data performed by Collins et al. (1981), and in our own unpublished experiments, the lowest χ^2 values were obtained when Fe was assigned to these sites, suggesting some degree of cation order in this phase.

This paper investigates the short-range and long-range structural changes in bornite as a function of temperature, using differential scanning calorimetry (DSC) to study the thermal anomalies and in-situ high-resolution neutron powder diffraction to determine the changes in superlattice intensity and lattice parameters. In particular, we focus on the nature and the temperature dependence of the two phase transitions and so on the relationship between them. The characterization of phase transitions and the thermodynamic behavior of the various polymorphs of bornite is of potential application in the modeling of ore deposit formation, because most important bornite-bearing mesothermal deposits are formed at temperatures above that of the low-intermediate transtion.

EXPERIMENTAL METHODS

Sample collection and characterization

We used two natural samples from mesothermal deposits where bornite is a major copper ore and occurs in large, relatively pure masses. One sample originated from the 4600′ level, Magma Mine, Superior, Arizona, and the other was collected from a large bornite-chalcopyrite-hematite vein at the 39LJ59 Grizzly Access, Olympic Dam Mine, Roxby Downs, South Australia. Both samples were trimmed of visible contaminating phases, and when examined using reflected light microscopy proved to be remarkably pure. Trace amounts of digenite ($Cu_{8.9}Fe_{0.1}S_4$) and chalcopyrite ($CuFeS_2$) were noted in the Magma Mine sample, whereas the Olympic Dam sample contained only trace chalcopyrite. Microprobe analyses (Table 1) using analytical conditions detailed in Grguric and Putnis (1998) show both samples to be near stoichiometric.

Thermal analysis and hysteresis measurements

We used a Perkin-Elmer DSC 7 differential scanning calorimeter (Grguric and Putnis 1998). Hand-ground chips measuring 3 mm across and 0.5–0.8 mm thick and weighing 25 ± 2 mg were prepared from the samples, avoiding areas visibly contaminated with other phases. Each sample chip was weighed to a precision of 0.002 mg and placed in an Al sample tray, which was inserted into the calorimeter together with an empty Al reference tray. The sample environment in the calorimeter was purged with a constant flow of dry N_2 gas at 1 atm pressure. Each DSC analytical cycle consisted of an up-temperature scan at 10 °C/min from 50 to 300 °C followed by a down-temperature scan back to 50 °C at 5 °C/min. Temperature and transition enthalpy calibration was performed using the onset and area of endothermic melting peaks of ultra-pure In (156.60 °C; 28.45 J/g) and Sn (231.88 °C; 60.46 J/g), following the two-point calibration routine described by Callanan and Sullivan (1986). The quoted temperatures of the transitions in bornite correspond to the peaks of the thermal anomalies.

Chips from the Olympic Dam sample were used in a series of experiments on the thermal hysteresis of the transition peaks. The heating rate of the up-*T* scans was fixed at 10 °C/min from 50 to 300 °C followed by a down-*T* scan back to 50 °C in which the cooling rate was varied in a series of experiments from 1 to 20 °C/min. We estimate the systematic error for all DSC temperature measurements was in the region of $\pm$ 1–2 °C or better.

Neutron diffraction analysis

Approximately 2 cm³ of each bornite sample was used for neutron diffraction analysis. After being finely ground under acetone in an agate mortar and pestle, the powder was sealed under vacuum together with a silica wool plug in high-purity Spectrosil silica-glass capsules. Diffraction measurements were performed on the high-resolution neutron powder diffractometer (HRPD) at the ISIS spallation source, Oxfordshire (Johnson and David 1985; Ibberson et al. 1992). The sample capsules were inserted into a cylindrical vanadium sample can and fitted to the central stick of the diffractometer together with a cartridge heater. Temperature measurements were made using a rhodium and iron thermocouple mounted along the edge of the sample can and the environment of the sample
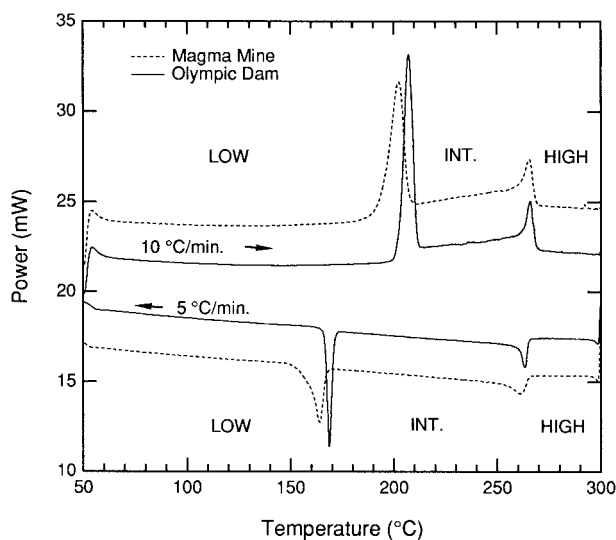
FIGURE 1. DSC scan profiles of the two bornite samples used in this study. Up- and down-T scan rates are 10 and 5 °C/min, respectively. Peak just above 50 °C is due to initial thermal capacity mismatch between the sample and reference containers. Vertical positions of scans have been translated for clarity.

TABLE 1. Representative electron microprobe analyses

	Magma Mine, Az.	Olympic Dam, Aust.
Cu (wt%)*	63.38	63.66
Fe (wt%)	10.96	11.08
S (wt%)	25.55	25.26
Total (wt%)	99.88	100.0
Formula	$Cu_{5.01}Fe_{0.99}S_{4.00}$	$Cu_{5.04}Fe_{1.00}S_{3.96}$
M/S	1.498	1.523
Cu/Fe	5.083	5.050

Note: Wavelength dispersive methods were used. Approximately 20 analyses were performed on each sample.
* Chalcocite standard used for Cu; pyrite for Fe and S.

tank was maintained at a vacuum of approximately 10^{-1} torr to minimize air scattering. The samples were equilibrated at each temperature for 5 min and then data collected for 15 min before moving on the next temperature setting. Measurements were made in steps of between 5 and 10 °C. The temperature of the furnace during the measurement was stable to within ± 2 °C. The absolute accuracy of the quoted furnace temperature is estimated as ± 10 °C, due to the large sample size and the position of the thermocouple.

Diffraction data were collected in two neutron time-of-flight (TOF) windows spanning 35–120 ms and 85–165 ms, corresponding to d-spacing ranges of 0.72–2.49 Å and 1.76–3.42 Å, respectively. All measurements were made with the diffractometer at the 1 m position, giving an intrinsic resolution of $\Delta d/d = 8 \times 10^{-4}$ for the entire TOF range (Knight 1996). The data were normalized to the incident neutron spectrum, and the background subtraction and detector efficiency corrections made using the program VA_COR (Ibberson et al. 1992), which uses a diffraction pattern of metallic vanadium. Superstructure peak intensities were measured using the ISIS in-house program PRGFIT, and cell parameters were obtained by performing full-pattern fits on the TOF spectra.

RESULTS

Differential scanning calorimetry

The up-T DSC scans of both bornite samples (Fig. 1) show the distinct endothermic peaks at approximately 200 and 265 °C noted by earlier workers (Kanazawa et al. 1978; Robie et al. 1994) and associated with the low-intermediate (L-I) and intermediate-high (I-H) transitions, respectively. The onset of the I-H transition is gradual

and appears to overlap with the L-I transition, as shown by the raised baseline on the high-temperature side of the L-I transition peak and the smooth up-temperature increase throughout the whole range of the intermediate structure. The slight differences in both the onset temperatures and peak profiles of the L-I transition anomalies between the two samples have been discussed by Grguric and Putnis (1998). The peak of the thermal anomaly occurs at a temperature of 202.4 °C in the Magma Mine bornite and 207.2 °C in the Olympic Dam specimen. The Magma Mine sample has a slightly lower M:S ratio relative to the Olympic Dam sample (Table 1) implying a larger metal vacancy population, which may account for the differences in onset temperatures. The similar Cu:Fe ratios of the two samples accounts for the lack of significant difference in their I-H transition peak temperatures (265.5 °C), following the T_c-Cu:Fe relationship found for this transition (Grguric and Putnis 1998). Integration of the areas of the transition peaks gives enthalpies of 4.5 ± 0.2 kJ/mol and 2.5 ± 0.2 kJ/mol for the L-I and I-H thermal anomalies, respectively (average of both samples).

In the down-T scans (Fig. 1) there is a slight hysteresis of a few degrees associated with the H-I transition, as well as a difference in the peak profiles for the two samples. The H-I transition is associated with a long down-T tail, reaching the I-L transition. We return to this observation when describing the diffraction data, as it suggests that the onset of the I-L transition may be associated with the slow completion of the H-I transition. The I-L transition shows a much greater hysteresis than the H-I transition, 38 °C in both samples. The shape of the peak and the hysteresis is characteristic of a first-order transition. This transition is much sharper than the H-I transition, especially in the Olympic Dam sample. Again the difference between the peak profiles of the I-L transitions of the two samples, and in particular the smearing observed in the Magma Mine down-T profile, may be due to a higher defect concentration in this sample (Levanyuk et al. 1979; Strukov et al. 1980; Salje et al. 1991).

To determine the effect of cooling rate on the hysteresis for the two transitions, experiments were carried out over a range of cooling rates (Fig. 2). The nature of the two transitions differ. The degree of thermal hysteresis for the
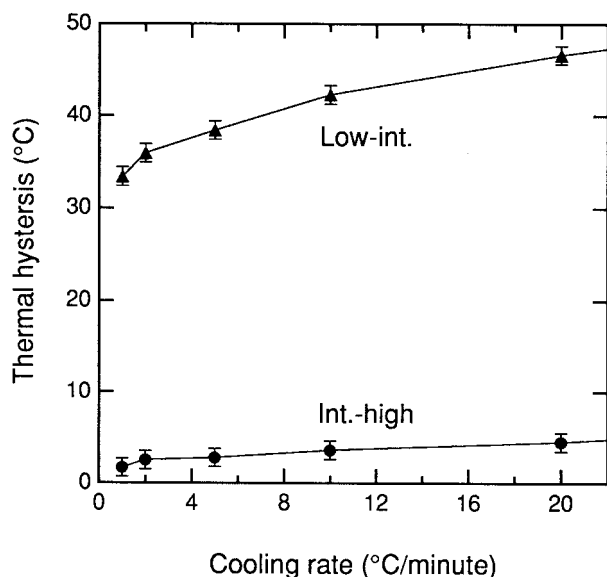
FIGURE 2. Hysteresis of thermal anomalies associated with both phase transitions in Olympic Dam bornite measured using DSC. The up-*T* heating rate was fixed at 10 °C/min for all experiments.

FIGURE 3. Normalized neutron TOF diffraction patterns of Olympic Dam bornite collected at 50 (bottom), 210, and 270 °C (top). Data points have been binned in groups of four.

L-I transition increases more with cooling rate compared with the I-H transition.

Neutron diffraction

The neutron powder diffraction data were used to determine the changes in the lattice parameters as a function of temperature on heating and cooling, as well as to measure the intensity changes in the superlattice peaks associated with the intermediate and low temperature phases. Diffractometer traces of bornite at three temperatures (Fig. 3) illustrates the disappearance of successive sets of superlattice reflections at each phase transition. The changes in the cell parameters (Fig. 4) indicate the nature of each transition. In the up-*T* experiments the transition from orthorhombic to cubic (2*a*) symmetry at 190 °C (L-I) is clearly a first-order process and can be compared with the thermal anomaly at 202 °C measured in the DSC. This apparent temperature difference is likely due to the different experimental configurations in each case (sample size, heating rate, thermocouple position, etc.). The L-I transition is immediately followed by a gradual non-linear increase in the average cell-edge of the intermediate phase. The cell-edge profile appears to have discontinuities at around 250 and 275 °C. The DSC anomaly for the I-H transition in the up-*T* scan is at 265 °C.

The behavior of the lattice parameters during cooling differs from those for heating for several reasons. First, the high-temperature phase appears to persist down to about 230 °C, where the discontinuity marks the formation of the intermediate phase. The DSC scan shows the H-I transition anomaly at about 261 °C. Given that the DSC data for the H-I transition shows virtually no hys-
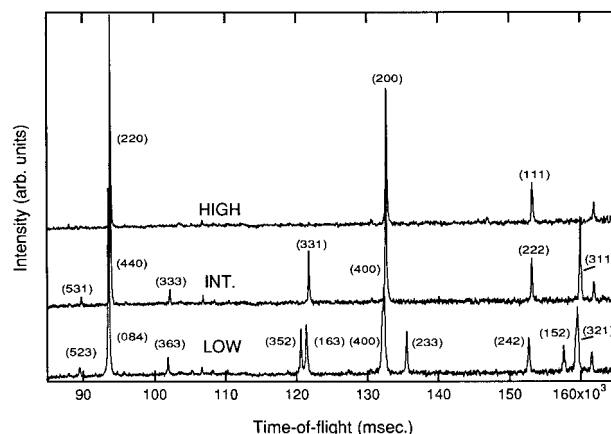
teresis at slow scan rates, this apparent hysteresis in the transition measured from diffraction data is most likely due to the effect of fine scale anti-phase domain formation during cooling below the H-I transition temperature. We return to this issue below.

The I-L transition on cooling is marked by a clearly defined first-order change in the lattice parameters at 160 °C (Fig. 4b). This is 30 °C lower than the up-T L-I transition and reflects a real hysteresis, also shown in the temperatures of the DSC peak for this transition. Thus for the L-I transition there are no short-range order effects that make the DSC anomalies different from the transition temperatures determined by neutron diffraction. Another observation that we return to below is that despite the 30 °C temperature difference between the L-I and I-L transitions on heating and cooling, they occur at the same value of the lattice parameter of the intermediate phase ($a = 5.49$ Å).

Several relatively high-intensity superstructure peaks were observed in both TOF windows of the neutron diffraction spectra (Fig. 3). Plots of superlattice peak intensity against temperature are presented in Figure 5. The superlattice peaks are indexed on the basis of their respective supercells. Thus the (321) and (363) superlattice reflections indexed on the low-temperature 2*a*4*a*2*a* superstructure become the (311) and (333) superlattice reflections, respectively, in the 2*a* superlattice of the intermediate phase; the (233) superlattice reflection in the low-temperature phase is lost in the intermediate phase (Fig. 3). In Figure 5 the $(321)_{low} \rightarrow (311)_{int}$ and $(233)_{low}$ reflections were measured on heating and the $(333)_{int} \rightarrow (363)_{low}$ and $(233)_{low}$ reflections measured on cooling.

The loss of the long-range 2*a*4*a*2*a* superstructure up-*T*, as indicated by the disappearance of the (233) reflection occurs over a short-temperature range in the vicinity of 200 °C, consistent with a first-order process. Comparison with Figure 1 shows that this loss of long-range order coincides with the thermal anomaly for this transition.
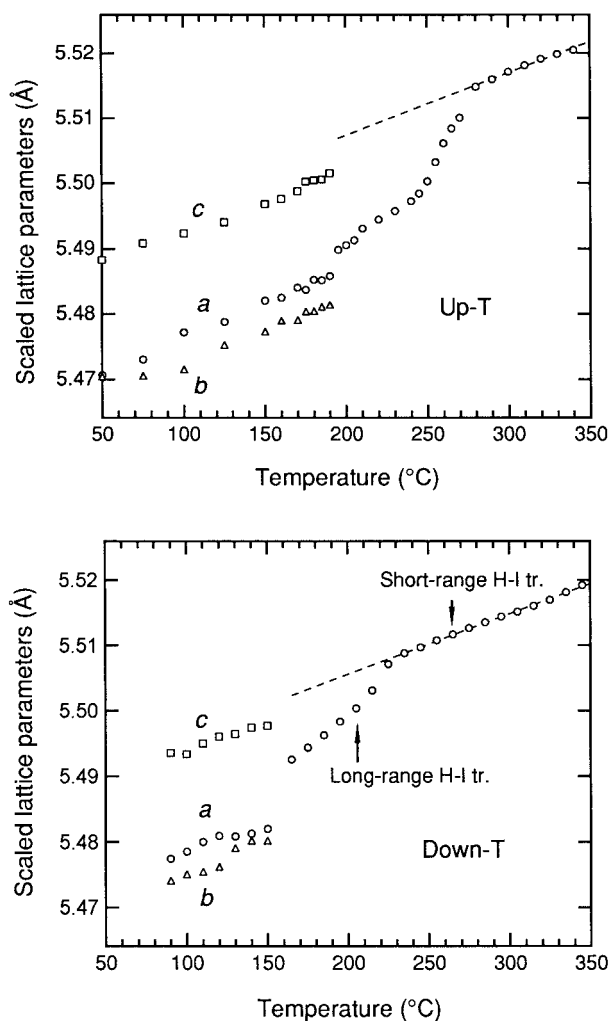
Figure 4. Up- and down-T lattice parameters for Magma Mine bornite. Low and intermediate polymorph lattice parameters were scaled to the cell-edge of the high polymorph for clarity. Data obtained from whole pattern fits to the time-of-flight spectra. The short-range T_c refers to the DSC anomaly whereas the long-range T_c refers to the onset of superlattice intensity. Dashed lines show the extrapolation of the high-phase lattice parameters used to calculate the spontaneous strain in the intermediate phase. Errors on the data are less than the size of the symbols.

Figure 5. Plots of superstructure peak intensity variation during (**a**) heating and (**b**) cooling. The reflections are indexed on the relevant superlattice. The (233) reflection is a superlattice peak of the low phase, which does not exist in the intermediate phase. The (321) and (363) reflections are low-phase superlattice reflections that also exist in the intermediate phase, as (311) and (333) respectively.

The intensity of the (321) superstructure peak also reduces as the contribution from this long-range order is lost. At temperatures above the L-I transition, the remaining intensity in the reflection, now indexed as (311), continues to fall until it is lost at about 250 °C. The structural changes associated with the I-H transition (shown by the reduction in 311 superlattice intensity) begin just as the L-I transition is completed, in agreement with the DSC data.

The down-T behavior of the superlattice intensities also demonstrates that the intensity in the (333) superlattice peak, associated with ordering in the intermediate form,
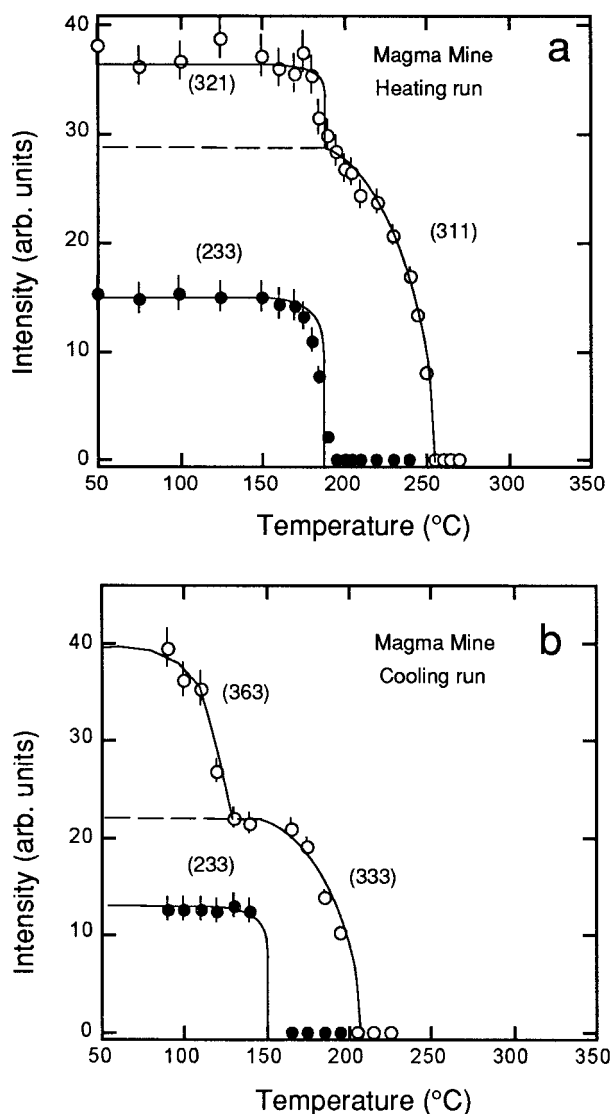
just becomes saturated at the temperature where the I-L transition takes place. Also the hysteresis associated with the I-L transition is again clearly evident by comparing Figures 5a and 5b.

Although some differences exist in the exact temperatures and the detailed form of the superlattice intensity-temperature curves as well as the variation in lattice parameters for the Magma Mine and Olympic Dam bornite samples, the same pattern emerges. The L-I phase transition is first-order whereas the I-H transition is continuous. Allowing for the differences in sample heating rate used during the collection of the neutron diffraction and

DSC data, the transition temperatures for the L-I transition measured in both experiments are essentially the same. Thus the loss of short-range and long-range order is simultaneous. During cooling, the short-range order associated with the H-I transition, marked by the DSC anomaly, occurs some 50 °C higher than the onset of long-range order associated with the appearance of the $2a$ superlattice peaks. The I-L transition exhibits a true hysteresis seen in both the DSC anomaly and the appearance of the $2a4a2a$ superlattice peaks, both short- and long-range order occurring simultaneously.

Thermodynamics of the I-H transition

The thermodynamic nature of the I-H transition can be determined by examining the temperature evolution of the lattice parameters and the superlattice peak intensities in detail. According to the Landau theory of phase transitions, the state of cation order in a material is described by an order parameter, Q, which varies smoothly between $Q = 0$ in the disordered state (i.e., when Cu, Fe, and vacancies are randomly distributed over the eight tetrahedral sites of the cubic close packed S lattice), and $Q = 1$ in the fully ordered intermediate structure (i.e., when the cations and vacancies are fully segregated into the M1- and M2-type cubes) (Landau and Lifshitz 1980; Salje 1990). The temperature dependence of Q follows a power law of the form:

$$Q \propto |T - T_c|^\beta$$

where T_c is the transition temperature, $\beta = 0.5$ for a second-order transition, and $\beta = 0.25$ for a tricritical transition. The relationship between Q and the macroscopic properties of the material are strictly defined by well established symmetry arguments. For the I-H transition, which involves a doubling of the unit cell with no change in point group symmetry, we expect both the superlattice intensities and the spontaneous strain (see definition below) to be proportional to Q^2.

The spontaneous strain, e_{ij}, associated with the I-H transition is a second rank tensor describing the relationship between the unit cell of the intermediate phase and the hypothetical unit cell of the high phase extrapolated to the temperature of interest (to account for thermal expansion) (Salje 1990). Because both the intermediate and high phases are described relative to the same set of cubic axes, there are no off-diagonal terms in the strain tensor, and the three diagonal terms (e_{11}, e_{22}, and e_{33}) are equal:

$$e_{11} = e_{22} = e_{33} = \frac{a - a_0}{a_0}$$

where a is the scaled lattice parameter of the intermediate phase and a_0 is the extrapolated lattice parameter of the high phase. The thermal expansion of the high phase is approximately linear (as can be seen from the high temperature data points in Fig. 4). The lattice parameter of the high phase was extrapolated (dashed lines in Fig. 4) into the stability field of the intermediate phase by fitting a straight line via least squares to the data points above
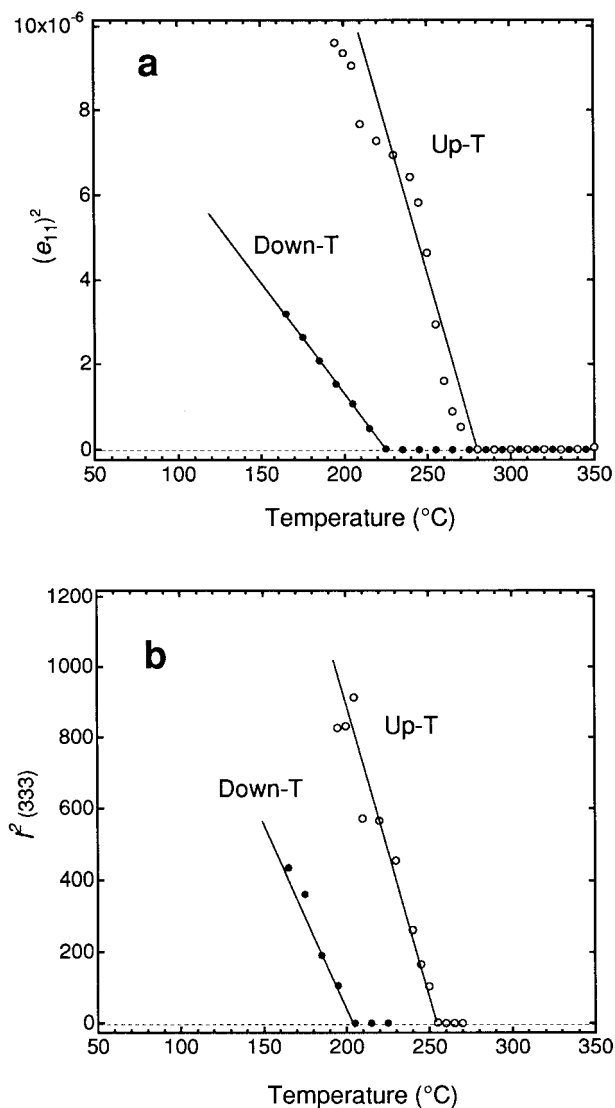

FIGURE 6. (**a**) Linear fits to e_{11}^2 vs. temperature for Magma Mine bornite associated with the I-H transition on heating and H-I on cooling. Calculation of e_{11} was performed using lattice parameter data in Figure 4. Scatter in up-T data may be due to mechanical strain induced during sample grinding (annealed out on further heating). (**b**) Plots of the square of the intensity of the (333) superlattice reflection derived from the same diffraction data as in (**a**).

the I-H transition temperature (approximately 275 °C for the up-T data and 225 °C for the down-T data). The lattice parameter of the intermediate phase is lower than that for the extrapolated high phase. This decrease in unit-cell volume is associated with the more efficient packing of cations and vacancies in the ordered intermediate phase in comparison to the disordered arrangement in the high phase.

Figure 6 suggests that each of the square of the spontaneous strain (e_{11}^2) and the square of the (333) superlattice intensity (I^2) vary linearly with temperature with some

degree of scatter. This is most clearly seen in the down-*T* strain data in Figure 6a. Scatter in the up-*T* strain data may be due to mechanical strain induced during sample grinding, which is annealed out on heating. Scatter in the intensity data is due to experimental uncertainty. Because both the strain and the superlattice peak intensity couple to the square of the order parameter, we conclude that Q^4 is linear with temperature and that the I-H transition is tricritical in character (i.e., $\beta = 0.25$). This information can in principle be used to determine the correct form of the free energy potential associated with the transition (Salje 1990).

Although the general temperature dependencies of the spontaneous strain and the superlattice intensity are consistent with each other (both suggesting a tricritical phase transition), Figure 6 shows that there is a difference of around 20 °C between the transition temperatures measured using strain and those measured using superlattice intensity, even though both parameters have been obtained from the same neutron diffraction data set. In addition, there is a obvious hysteresis in transition temperature between up-*T* and down-*T* measurements. No such hysteresis was measured for the H-I transition using DSC (Fig. 1). The origin of these apparent discrepancies requires careful consideration of the development of short- and long-range order during heating and cooling, discussed below.

DISCUSSION

On the basis of the bornite polymorph structural determinations of Koto and Morimoto (1975) and Kanazawa et al. (1978), the H-I transition involves a combination of vacancy clustering and cation ordering. The requirement for a long-range rearrangement of the cations and vacancies from the random distribution in the high phase suggests that the transition is a gradual ordering process dependent on diffusion kinetics. With that in mind we can interpret the temperatures of the transitions as measured by DSC and by neutron diffraction experiments in terms of the relative development of short-range and long-range order.

The transition from the high phase to the intermediate phase involves a doubling of the unit-cell edge along the *a, b,* and *c* crystallographic axis. Although there is no change in space group symmetry on doubling the cell (it is $Fm3m$ in both cases), the reduction in translational symmetry leads to the formation of anti-phase domains (Nord 1992). The crystal structure within an anti-phase domain is indistinguishable from that of adjacent domains. Each domain differs from its neighbors simply by a shift in origin, where the vector relating the origin of one domain to another is equal to one of the translational symmetry operations, which was lost during the transition. The number of physically distinguishable origins for the intermediate phase (and hence the number of domains expected) can be determined in this case from the ratio of the volumes of the unit cells of the intermediate and high phases (= 8). In a homogeneous defect-free crystal,

we would expect all eight domains to occur with equal probability. Adjacent domains are separated by a domain wall, the structure of which more closely resembles the disordered structure of the high phase than the ordered structure of the domains themselves (Putnis and McConnell 1980; Nord 1992).

We have demonstrated that the I-H transition is a continuous tricritical process. Hence the transition from the disordered high phase to an ordered intermediate phase containing anti-phase domains is expected to occur at a single transition temperature, with no intrinsic hysteresis. This is consistent with the thermal anomaly observed using DSC (Fig. 1). The small difference in the peak position of the thermal anomaly during heating and cooling is due to a combination of thermal lag in the calorimeter and kinetic lag due to diffusion of the metals and vacancies through the structure, and does not reflect intrinsic hysteresis of the kind associated with the I-L transition. In comparison, the I-H transition observed using neutron diffraction displays a hysteresis of around 55 °C (Fig. 6).

We can understand these apparent differences by noting that the DSC measures the thermal effects of the change in the cation distribution and is therefore not affected by any averaging over domains. Thus the transition temperature is a true record of the local order-disorder phase transition and shows no hysteresis. The neutron diffraction experiments measure the crystal structure averaged over many unit cells, and are therefore affected by the domain state in the intermediate phase. For an intermediate phase containing fairly coarse anti-phase domains (i.e., the volume of domains $\gg$ volume of domain walls), the crystal structure within each domain is identical to all other domains, and in the same orientation (there is no twinning associated with the transition). If the lattice parameter is averaged over the whole volume of the crystal then the average value is equal to the value within each domain. In this case, we expect spontaneous strain simultaneously developing with the intermediate phase as seen in the DSC.

For an intermediate phase consisting of very fine-scale anti-phase domains (i.e., volume of domains $\ll$ volume of domain walls), the average lattice parameter will be closer to that of the domain wall. Because the domain wall is relatively disordered, it will have a lattice parameter equivalent to the extrapolated high-temperature phase, and the apparent spontaneous strain is zero. We suggest that the suppression of the spontaneous strain on cooling is caused by the presence of such fine-scale anti-phase domains. These domains coarsen on cooling, leading to the observation of strain at lower temperatures. On reheating, or after long periods of time at low temperatures, the domains appear to be much coarser, as indicated by the fact that transition temperature measured on heating is much closer to the intrinsic transition temperature observed using DSC. Antiphase domain coarsening associated with the H-I transition in natural bornite has been previously observed using TEM (Putnis and Grace 1976).

The fact that the transition temperatures observed using

measurements of superlattice intensity during heating and cooling do not agree with those determined using spontaneous strain (Fig. 6) indicates that different structural criteria govern the appearance and disappearance of superlattice reflections. If we consider the coarse- and fine-scale domain structures discussed above, the structure factor for a superlattice reflection averaged over the whole crystal is zero in both cases if there are equal volumes of all eight possible anti-phase domains (i.e., the long-range order parameter is zero). The superlattice reflection only appears when the volume of one type of domain outweighs the volume of the others on a length-scale that is greater than the coherence length of the neutron beam used to perform the diffraction experiment (i.e., the long-range order parameter is non-zero). Such imbalances in the volume of domains may develop in areas where one domain is favored relative to the others due to the presence of compositional inhomogeneities, defects, or lattice strains.

A different apparent transition temperature can be derived from the strain data and the superlattice intensity data if many small antiphase domains form following the H-I transition. The average lattice parameter decreases, but the superlattice reflections are not observed until coarsening of the domains, as described above, occurs with further undercooling. This would give a lower transition temperature recorded from the superlattice intensity data than the spontaneous strain data, as observed.

During heating the opposite applies. After the loss of long-range order (and thus the loss of the superlattice peak) considerable short-range order can persist. All local domains of short-range order still have an additive affect on the lattice parameters, and only after this short-range order is lost will the true lattice parameter associated with the high-temperature phase be attained. The heterogeneity in the development of long-range order on cooling was noted by Putnis and Grace (1976) in TEM experiments where diffuse streaking along <111> was observed coexisting with sharp $2a$ diffraction reflections on slow cooling.

The dependence of the apparent transition temperature of the long-range H-I transition on domain size and volume may also account for the different transition temperatures measured in the two bornite samples. A difference in defect population may be instrumental as defects can effectively pin domain walls (Salje 1990). Because the two samples have different metal:sulfur ratios (Table 1), which in the bornite structure relates directly to the vacancy population, this compositional variation may be responsible for the difference in T_c. Trace elements and the dislocation density (Hull and Bacon 1984) may also play a significant role in this process.

The I-L transition involves further modifications of the intermediate phase, including ordering of the vacancies and copper atoms in the M1 cubes to form zinc blend-type cubes in two different orientations as well as the possibility that Cu, Fe ordering takes place in the antifluorite type M2 cubes (Koto and Morimoto 1975). It is

therefore reasonable to expect that this transition may be triggered by the attainment of a certain degree of order in the intermediate phase. The long tail in the DSC anomaly associated with the intermediate phase (Fig. 1) as well as the fact that the intermediate phase superlattice peak intensity may need to be fully saturated at the onset of the I-L transition (Fig. 5) suggests that the temperature of the I-L transition may be dependent on the kinetics of the H-I transition. In other words, cation/vacancy ordering in the M1 cubes cannot begin until the long-range distribution of these cubes is fully established in the intermediate phase. This threshold degree of order at which the low phase can form might also be defined by the lattice parameter of the intermediate phase ($a = 5.49$ Å) at which the I-L and L-I transitions take place. This value was found to be identical for both samples, despite the transition temperature difference.

The intermediate phase is quenchable, but the I-L transition can occur within several days at room temperature (Morimoto and Kullerud 1961) as well as during grinding of the quenched material (Allais and Curien 1970). This suggests that no long-range diffusion process is involved and that the activation energy for the transition is small. The apparently large hysteresis in the I-L transition may be due to the rate at which the intermediate phase achieves a sufficiently high degree of order, rather than any inherent kinetics of the I-L transition. Extrapolating the hysteresis curve for this first-order transition (Fig. 2) to typical cooling rates associated with water-quenching (>100 °C/s) demonstrates how this could occur.

REFERENCES CITED

Allais, G. and Curien, H. (1970) Physical and crystallographic properties of bornite, Cu₅FeS₄ and digenite Cu₇S₄. In S.C. Jain and L.T. Chadderton, Eds., Nonmetallic Crystals. Gordon and Breach, London.

Allen, F.M. (1992) Mineral definition by HRTEM: problems and opportunities. In Mineralogical Society of America Reviews in Mineralogy, 27, 289–333.

Berger, R. and Bucur, R.V. (1996) Potentiometric measurements of copper diffusion in polycrystalline chalcocite, chalcopyrite and bornite. Solid State Ionics, 89, 269–278.

Callanan, J.E. and Sullivan, S.A. (1986) Development of standard operating procedures for differential scanning calorimeters. Review of Scientific Instruments, 57, 2584–2592.

Collins, M.F., Longworth, G., and Townsend, M.G. (1981) Magnetic structure of bornite, Cu₅FeS₄. Canadian Journal of Physics, 59, 535–539.

Grguric, B.A. and Putnis, A. (1998) Compositional controls on phase transition temperatures in bornite: a DSC study. Canadian Mineralogist, 36, 215–227.

Grguric, B.A., Dove, M.T., Harrison, R.J., and Putnis, A. (1996a) A neutron diffraction study of phase transitions and superstructures in bornite Cu₅FeS₄. Terra Nova Abstract Supplement 1, Vol. 8, 25.

Grguric, B.A., Dove, M.T., Harrison, R.J., and Putnis, A. (1996b) Phase

transitions and superstructuring in natural bornite (Cu_5FeS_4). The ISIS Facility Annual Report, 2, A192.

Hull, D. and Bacon, D.J. (1984) Introduction to dislocations. Pergamon Press, 257.

Ibberson, R.M., David, W.I.F., and Knight, K.S. (1992) The high resolution powder diffractometer (HRPD) at ISIS—a user guide. Rutherford-Appleton Laboratory Report RAL-92–031.

Johnson, M.W. and David, W.I.F. (1985) The high resolution powder diffractometer at the SNS. Rutherford-Appleton Laboratory Report RAL-85–112.

Kanazawa, Y., Koto, K., and Morimoto, N. (1978) Bornite (Cu_5FeS_4): stability and crystal structure of the intermediate form. Canadian Mineralogist, 16, 397–404.

Knight, K.S. (1996) A neutron powder diffraction determination of the thermal expansion tensor of crocoite ($PbCrO_4$) between 60K and 290K. Mineralogical Magazine, 60, 963–972.

Koto, K. and Morimoto, N. (1975) Superstructure investigation of bornite, Cu_5FeS_4, by the modified partial Patterson function. Acta Crystallographica, B31, 2268–2273.

Landau, L.D. and Lifshitz, E.M. (1980) Statistical Physics. Pergamon Press, Oxford, U.K.

Levanyuk, A.P., Osipov, V.V., Sigov, A.S., and Sobyanin, A.A. (1979) Change of defect structure and the resultant anomalies in the properties of substances near phase transition points. Soviet Physics JETP, 49, 176–188.

Morimoto, N. (1964) Structures of two polymorphic forms of Cu_5FeS_4. Acta Crystallographica, 17, 351–360.

Morimoto, N. and Kullerud, G. (1961) Polymorphism in bornite. American Mineralogist, 46, 1270–1282.

———(1966) Polymorphism on the Cu_5FeS_4-Cu_9S_5 join. Zeitschrift für Kristallographie, 123, 235–254.

Nord, G.L. Jr. (1992) Imaging transformation-induced microstructures. In Mineralogical Society of America Reviews in Mineralogy, 27, 455–508.

Pierce, L. and Buseck, P.R. (1978) Superstructuring in the bornite-digenite series: a high-resolution electron microscopy study. American Mineralogist, 63, 1–16.

Putnis, A. (1992) Introduction to mineral sciences, 457 p. Cambridge University Press, Cambridge, U.K.

Putnis, A. and Grace, J. (1976) The transformation behaviour of bornite. Contributions to Mineralogy and Petrology, 55, 311–315.

Putnis, A. and McConnell, J.D.C. (1980) Principles of Mineral Behaviour, 257 p. Blackwell, Oxford, U.K.

Robie, R.A., Seal, R.R., and Hemingway, B.S. (1994) Heat capacity and entropy of bornite (Cu_5FeS_4) between 6 and 760K and the thermodynamic properties of phases in the system Cu-Fe-S. Canadian Mineralogist, 32, 945–956.

Salje, E.K.H. (1990) Phase transitions in ferroelastic and co-elastic crystals, 230 p. Cambridge University Press, Cambridge, U.K.

Salje, E., Bismayer, U., Wruck, B., and Hensler, J. (1991) Influence of lattice imperfections on the transition temperatures of structural phase transitions: the plateau effect. Phase Transitions, 35, 61–74.

Strukov, B.A., Taraskin, S.A., Minaeva, K.A., and Fedorikhin, V.A. (1980) Critical phenomena in perfect and imperfect TGS crystals. Ferroelectrics, 25, 399–402.